What your eye tells your brain

Katja Reinhard[1,2,3] *& Thomas A. Münch*[1,4]

[1] Retinal Circuits and Optogenetics, Centre for Integrative Neuroscience and Bernstein Center for Computational Neuroscience, University of Tübingen, Otfried-Müller-Str. 25, 72076 Tübingen, Germany

[2] Neuroscience Graduate School, University of Tübingen, Österbergstraße 3, 72074 Tübingen Germany

[3] Current address: Neuro-electronics Research Flanders, Kapeldreef 75, 3001 Leuven, Belgium

[4] Institute for Ophthalmic Research, University of Tübingen, Elfriede-Aulhorn-Straße 7, 72076 Tübingen, Germany

Corresponding author

Thomas A. Münch
Retinal Circuits and Optogenetics
Werner Reichardt Centre for Integrative Neuroscience
Otfried-Müller-Str. 25
72076 Tübingen
Germany

thomas.muench@cin.uni-tuebingen.de
Phone: +49 (0)7071 29-89182
Fax: +49-7071-29 25007

Abstract

The retinal output is the sole source of visual information for the brain. Studies in non-primate mammals estimate that this information is carried by several dozens of retinal ganglion cell types, each informing the brain about different aspects of a visual scene. Even though morphological studies of primate retina suggest a similar diversity of ganglion cell types, research has focused on the function of only a few cell types. In human retina, recordings from individual cells are anecdotal. Here, we present the first systematic ex-vivo recording of light responses from 342 ganglion cells in human retinas obtained from donors. We find a great variety in the human retinal output in terms of preferences for positive or negative contrast, spatio-temporal frequency encoding, contrast sensitivity, and speed tuning. Some human ganglion cells showed similar response behavior as known cell types in other primates, while we also recorded light responses that have not been described previously. This first extensive description of the human retinal output should facilitate interpretation of primate data and comparison to other mammalian species, and it lays the basis for the use of ex-vivo human retina for in-vitro analysis of novel treatment approaches.

Introduction

Vision starts in the retina, a highly structured part of the central nervous system. The retina performs important signal processing: the incoming images are captured by the photoreceptors, analyzed and split into parallel information streams by retinal circuits, and sent along the optic nerve to higher visual brain centers. Each of the parallel information streams is embodied by a type of ganglion cell and informs the brain about a particular aspect of the visual scene [1]. The non-primate mammalian retina contains over 40 of these different information streams, which can be distinguished based on both functional and morphological criteria [2–7].

One striking feature of retinal architecture is that each ganglion cell type tiles the retina so that each feature can be extracted at each location in the visual field. Nevertheless, regional specializations do exist, for example the fovea of the primate retina, a region of very high visual acuity. The foveal region consists almost exclusively of four retinal ganglion cell types, the ON and OFF parasol cells and the ON and OFF midget cells [8–10], which account for 50-70% of all ganglion cells in the primate retina [11]. Functional studies using non-human primates have often focused on these four most abundant retinal ganglion cell types [12–17]. Morphological studies of the complete primate retina, on the other hand, describe a similar variety in ganglion cell types as found in the non-primate retina with at least 17 morphologically identified types [11,18–21]. However, functional studies of these non-foveal ganglion cell types in non-human primates have been limited to a set of 7 types [14,22–27], and physiological assessment of the *human* retina on the level of individual cells is anecdotal [28,29].

In this study, we performed a survey of ganglion cell function in the non-foveal human retina. We applied multi-electrode array (MEA) recordings to ex-vivo retinas obtained from enucleation patients and recorded light-driven activity from dozens of human ganglion cells in parallel. MEAs have been successfully used in previous studies to characterize the retinal

output in various animal models [4,12,30–35]. Our data represents the first systematic recording of light responses from a large population of ganglion cells in human retina. In addition to providing an overview of the spectrum of light responses in the human retina, we compare the representation of the spatio-temporal stimulus space by human ganglion cells with published data from non-human primate retina and results from psychophysical studies.

Results

Human retinas were obtained from patients who had to undergo enucleation of one eye due to a uveal tumor. Retinal pieces (~ 3 x 3 mm²) were placed ganglion cell-side down onto multi-electrode arrays and responses to a set of light stimuli were recorded at photopic light intensities. Individual stimuli (gray-scale images) spanned at most 3 log units of brightness. Spikes were assigned to individual units (presumably retinal ganglion cells) during an offline, semi-manual spike sorting process based on principal component analysis of spike waveforms. Only clearly sortable units were considered for analysis (see Method section for details). In total, we obtained the spiking activity of 342 light-responsive single units in 15 retinal pieces obtained from 10 human retinas (Table 1).

Response properties across the population

We aimed at characterizing the diversity of the output of the human retina with different visual stimuli (Fig. 1). We used drifting-grating stimuli to characterize the encoding of the spatio-temporal space (Fig. 1A). Of the 342 light-responsive cells, 86% responded to these stimuli (Fig. 1E). As a population, the recorded cells responded to a large spatio-temporal stimulus space including all tested spatial frequencies (100-4000 µm spatial period on the retina, corresponding to 2.66-0.07 cycles per degree (cyc/°)) and temporal frequencies (1-8 Hz) with an overall preference for stimuli of 500-4000 µm retinal size (0.53-0.07 cyc/°) and moving with 2-8 Hz (Fig. 2A). Figure 2A shows the response strength averaged across all recorded cells to the 24 different sinusoidal drifting gratings. To obtain the displayed heat-

map, the amplitude in the Fourier Transform of the cells' responses at the stimulus frequency was taken as response strength and normalized for each cell across the 24 grating stimuli. The distribution of preferred spatial and temporal frequencies per cell are shown in Figure 2B (maximum out of the 24 drifting-grating combinations). While the recorded ganglion cells showed responses to a broad range of spatial and temporal frequencies (Fig. 2A), they mostly responded best to coarse gratings (Fig. 2B left) and higher temporal frequencies (Fig. 2B right).

Temporal frequency preferences were further measured with a full-field frequency ramp ("chirp" stimulus, Fig. 1B top) which has proven to be an excellent stimulus to classify the behavior of retinal ganglion cells [2], and which drove activity in 41% of our analyzed cells. Here, response strength was defined as the ratio of the Fourier Transform of the cells' response and the Fourier Transform of the stimulus. This chirp stimulus confirmed a general preference of the human retinal output for higher temporal frequencies (Fig. 2C).

Bars moving with different velocity (Fig. 1C) were used to test for the preferred speed of ganglion cells and elicited clear responses in 11% of all cells. The distribution of the median preferred speeds (50% of the cumulative sum of the response amplitudes) was rather wide, ranging from bars moving between 2 and 8 mm/s (7.5 to 30 °/s) in different ganglion cells (Fig. 2D).

Finally, response polarity was tested with full-field contrast steps (Fig. 1D). Over a third of the recorded cells responded consistently to this stimulus. Of those cells, 46% responded solely to positive full-field contrast-steps (ON-responses), 35% showed responses to negative contrast steps (OFF-responses), and the remaining 19% responded to both (ON-OFF-responses; Fig. 2E).

Diversity in the output of human retina

One hallmark of the retina is the separation of visual information into different information streams embodied by distinct ganglion cell types. When analyzing individual cells, we found a wide range of response properties to our set of light stimuli, illustrated with 16 example cells in Figure 3. These example cells span the range of observed response polarity and transiency, spatio-temporal preferences, contrast sensitivity, and responsivity to local stimuli. For the following description, we group these cells based on their responses to full-field contrast steps (column 1 in Fig. 3), with cells responding only to positive contrast steps (ON-cells) in Figure 3A, cells responding exclusively to negative contrast steps (OFF-cells) in Figure 3B, and cells responding to both (ON-OFF cells) in Figure 3C.

<u>ON-cells</u>: The cell A_1 in Figure 3 showed a very transient response to a positive contrast step (at the transition from black to gray full-field stimulation, column 1). It preferred coarse drifting-gratings with a high temporal frequency (columns 5 and 6), which is consistent with the steep increase in responsivity when shown a spatially homogeneous frequency ramp (column 4). The cell also responded to fast local stimulation by a moving bar (column 2). When probed with a contrast ramp, the activity of this cell was already modulated at relatively low contrast (column 3). A_2 is another transient ON-cell. Compared to the first cell, this cell responded well to a broader spectrum of temporal frequencies (columns 4 and 5).

Some recorded ganglion cells had very high spontaneous firing rates such as the cell A_3. Nevertheless, they precisely encoded high temporal frequency stimuli (columns 4 to 6) and showed selective and transient activity modulations to their preferred contrast step (column 1). In contrast to the first two cells, cell A_3 did not respond to local stimuli (column 2). High spontaneous firing rates were also found in the ON-cell A_4. In contrast to the cell A_3, it was strongly inhibited by negative contrast stimuli. Additionally, it responded well to 1-4 Hz stimuli, but not to 8 Hz (columns 4 and 5), responded better to finer gratings (column 5), and

followed well the complete contrast ramp, including the low-contrast phase of the stimulus (column 3).

The cell A_5 responded well to coarser drifting-gratings moving with 1-4 Hz (column 5). This cell showed a transient response peak to a positive contrast step, while a negative contrast step consistently caused a strong inhibition (column 1). While full-field drifting gratings elicited strong firing rate modulations (column 6), this cell did not respond to local moving bars (column 2).

<u>OFF-cells</u>: Four examples of transient OFF-cells are shown in Figure $3B_{1\text{-}4}$. Cell B_1 responded well to all moving bars up to speeds of 16 mm/s (column 2), cell B_3 preferred slower speeds, and the cells B_2 and B_4 did not respond at all to this more local stimulus. Stimulated with a full-field drifting-grating (columns 5 and 6), $B_{1\text{-}3}$ preferred higher temporal frequencies (4-8 Hz), and B_4 responded best to 2 Hz stimulation.

The sustained cells B_5 and B_6 both preferred low temporal frequencies (1-2 Hz) when probed with a drifting-grating stimulus (columns 5 and 6) or the chirp stimulus (column 4). The less sustained cell B_6 responded strongly to all moving bars, while the cell B_5 did not respond to this stimulus (column 2).

The OFF-cell B_7 exhibited a rebound or delayed response to positive contrast after an initial inhibition (column 1). The cell showed a preference for temporal frequencies around 4 Hz (columns 5 and 6) and higher contrast stimuli (column 3), and it responded well to all speeds of a moving bar (column 2).

<u>ON-OFF-cells</u>: Finally, ON-OFF cells may show rather sustained (cells C_1 and C_2, column 1) or transient responses (C_3, column 1). Some clearly prefer higher temporal frequencies (C_1, columns 4 to 6), others responded only to low frequencies (C_3, column 4). While the cell C_1 responded well to the whole contrast ramp (column 3), the other two example cells showed some activity modulation only to maximal contrast. Interestingly, the cell C_3 responded well

to temporal frequencies around 3 Hz when exposed to full-field stimulation (column 4), but did respond neither to drifting-gratings (column 4) nor moving bars (column 2).

Spatio-temporal properties of human ganglion cells correspond to psychophysical detection threshold

The responses to drifting or sign-inverting grating stimuli have often been used to characterize, identify, and compare different retinal ganglion cell types. We therefore explored the spatio-temporal stimulus space encoded by the human retina in more detail. The heat-map in Figure 2A (replicated in Fig. 4A) indicates that the mid-peripheral human retina responds well to all presented temporal frequencies and shows a general preference for coarser stimuli. To directly compare the human retina responses to published psychophysics and non-human primate data, we computed the spatial response curve of the whole population of recorded cells (Fig. 4A top and 4B). This was achieved by normalizing every cell's responses to each spatial frequency presented at its optimal temporal frequency, and then averaging these individual spatial response curves. In the same way, the temporal response curve was calculated (Fig. 4A left and 4C). The average spatial response curve dropped below 10% of its maximum for stimuli of 1.55 cyc/° and finer (Fig. 4A top). This in-vitro spatial threshold corresponds well to previously determined psychophysical detection thresholds in the mid-peripheral visual field (4 cyc/° at 14° visual angle and 2 cyc/° at 30°) [36].

Comparison to non-human primate data

Temporal and spatial frequency preferences have been used as the main parameter in several studies on non-human primate retina to characterize and identify different ganglion cell types [22,25,37–40]. In all non-human primate publications considered here for comparison with our human ganglion cell data, response strength has been given either as absolute number of spikes or as a normalized amplitude of the Fourier Transform of the cells' responses. We extracted the response curves from these publications (midget ganglion cells [37]; parasol ganglion cells [39], [41]; blue-yellow ganglion cells [39], [40]; upsilon ganglion cells [22]; melanopsin

ganglion cells [25]) and overlaid them with the population tuning curves obtained from our human ganglion cell data, as shown in Figure 4B and 4C. Both the average spatial response curve (Fig. 4B) and the average temporal response curve (Fig. 4C) for the human retina lie within the range of published data from different primate ganglion cell types.

The response properties of the example cells in Figure 3 suggest a great variety in the spatio-temporal preferences of the recorded human ganglion cells. We wondered whether we could identify the most common primate ganglion cell types, parasol and midget cells, in our data set. Proper classification of cell types would require morphological information and/or denser electrophysiological recordings to reveal mosaic formation. We thus did not aim to classify individual cells, but to identify groups of cells with similar response properties as known non-human primate cells. To group recorded cells from human retina, we directly compared normalized spatial and temporal response curves of individual cells to the published response curves obtained from macaque retina (see Method section for details).

<u>Cells resembling midget and parasol cells</u>: We did not detect any cell with a spatial response curve resembling the midget cells shown in Fig. 4B, with diminishing responses to very coarse drifting-grating stimuli. However, response curves of individual midget cells can vary substantially for very coarse stimuli (see Diller et al. 2004 [37]), and the spatial response curves of parasol and midget cells are very similar for finer spatial frequencies > 0.27 cyc/°. Furthermore, to our knowledge there is no published data comparable to ours on the temporal response behavior of midget cells. Therefore, the first group (Fig. 5A) contains cells that resemble both parasol and midget cells. All cells in this group have in common that they respond very well to grating stimuli of 0.07-1.33 cyc/° spatial frequency. Only one of the cells showed a very small detectable response to the finest grating of 2.66 cyc/°. This behavior is comparable to data from non-human primate parasol and midget cells which respond only weakly to such fine gratings. Similarly, the cells in this group follow the temporal response behavior of parasol cells with clear responses to all temporal frequencies.

Cells with broad spatio-temporal response profiles: A second group of cells (Fig. 5B) shows a similar behavior as group 1. However, in contrast to the first group, these cells responded strongly to the finest tested grating of 2.66 cyc/°. These cells thus show a very broad response profile with activity for most spatio-temporal combinations. To our knowledge, none of the published ganglion cells of non-human primates has a similar spatial response curve as these cells of the human retina.

Cells resembling small bistratified cells: The third group (Fig. 5C) contains human ganglion cells with similar spatio-temporal properties as the small blue-yellow or bistratified cell, the most abundant primate ganglion cell after parasol and midget cells. In terms of spatial response tuning, blue-yellow cells respond more weakly to drifting-grating stimuli of 1.33 cyc/° than parasol or midget cells (see also Fig. 4B and [39]). Accordingly, we grouped human cells in this third group that did not show detectable responses to such medium-fine gratings. The temporal response curve for the tested frequencies of 1-8 Hz is similar in all cell types discussed so far (Fig. 5A-C).

Other ganglion cells: The remaining 219 cells with robust responses to drifting-gratings are shown in Figure 5D. Many of these cells responded to a small subset of spatio-temporal combinations. The diversity is exemplified by the five cells highlighted in color. The purple cell has a similar spatial response curve as the group in Figure 5C, but does not respond to very slow gratings. The turquoise, orange and yellow cells have different types of rather narrow response spectra with the turquoise cell responding only to very slow stimuli, the orange cell strongly preferring wide gratings and the yellow cell responding best to slow and wide stimuli. Finally, the green cell has a very specific set of temporal and spatial frequency combinations that it responds to.

Ex-vivo human retinas are healthy

One potential problem when working with human retinas is the unclear health status of the donor tissue. We obtained retinas from donors between 42 and 89 years of age and with

different medical histories (Table 1). In addition to the variability introduced by the donors, several circumstances can damage the tissue and prevent light responses: Depending on the surgery conditions, the retina within the ligated eye bulb might have been exposed to longer periods without oxygen and nutrients (ischemia). Furthermore, because of the growing tumor, the retina might have been detached from the pigment epithelium prior to the surgery, which is particularly harmful to photoreceptors. In this study, we thus excluded all retinas exposed to ≥18 min of ischemia (control experiments with ischemic pig eyes have shown a strong decrease in light responses for longer ischemia times; data not shown, see also [42]). Further, we recorded only from retinal pieces in the opposite hemisphere of the eye bulb containing the tumor, and we included in the analysis only retinal pieces from which we could record light responses from at least 10 cells.

We performed several tests to assess the health status of the donor tissue. One hallmark of degenerating retina is tissue-wide oscillatory activity. Such oscillations have been observed in mouse models for retinitis pigmentosa [43] and have a frequency of approximately 9 Hz. In these retinas, each ganglion cell shows oscillatory activity which is synchronized across the whole tissue. We did not observe such oscillations in any of the recorded human retinas. Moreover, light-responsive cells (displayed as green circles in Fig. 6A) were distributed across the retinal piece, indicating good recording conditions.

Overall response strength is another indication of tissue health. We compared the response strength of the recorded cells in the human retina with published primate data, and computed the firing rate in the same way as previous publications on macaque retina [44]. We then extracted the peak firing rate for each cell to the full-field contrast steps (Fig. 3, column 1). Figure 6B shows the distribution of peak firing rates: many cells produced maximal responses of 20-90 Hz, but peaks could reach up to 180 Hz. Under comparable conditions (binary full-field noise), Uzzell & Chichilnisky report example cells with response peaks between <80 and

300 Hz [44]. The amplitude of the human response peaks reported here is hence in the same range as found in macaque retina.

Peak firing rates were not only comparable to published monkey data but were also stable throughout the experiments. Four retinal pieces were recorded for 2.5 hours and we computed peak responses averaged across blocks of 5 full-field contrast steps across the whole experiments. While some cells did not respond to this stimulus in the very beginning of the experiment, their peak firing rates were stable once they started responding (Fig. 6C_1). The responses at each time point (averaged across blocks of 5 steps) for an example cell are shown in Figure 6C_2. Similarly, spontaneous background spiking activity was stable across the full recording (Fig. 6D). Taken together, the recorded human retinas did not show typical signs of deteriorating or degenerated tissue and exhibited stable spontaneous and evoked activity.

Discussion

In this study, we describe light response properties of human retinal ganglion cells and find that these properties are very diverse. We found cells that responded only to positive contrast steps (ON cells), cells that responded only to negative contrast (OFF cells), and cells that encoded both positive and negative contrast (ON-OFF cells). The recorded human ganglion cells preferred different spatio-temporal stimulus frequencies and had distinct response properties when presented with local stimuli or contrast ramps. This diversity is consistent with the variety of cell types predicted by morphological classification in primate retina [11,19]. Our extensive dataset of 324 light-responsive ganglion cells provides an overview of the visual features routed by the human retina to the brain and suggests a similar richness of information processing in the primate retina as found in other mammals where recent studies estimate over 40 distinct retinal information streams [2,3].

There are three main aspects that might have led to an over-estimation of the diversity in our data set. First, most of our stimuli were full-field, and thus can reveal center-surround

interactions. These interactions can be very diverse across different cell types, such that full field stimuli might help to distinguish cell responses that may otherwise be very similar during local stimulation. The specific surround circuitry can depend strongly on the exact stimulus conditions including stimulus size [45] and absolute light level [45–47]. This dependency can contribute to an overestimation of the diversity of cell types. However, under our fixed stimulus conditions, it is not very likely that our large stimuli caused much artificial response variability. What is more, we might even have under-estimated the diversity in the responses as we probably have not recorded from cells that only respond to local stimuli. On the other hand, the diverse history of the donor tissue (age, health and genetic background of the donor, see the third point below), may have consequences for the surround contribution, such that full-field stimulation may exaggerate differing responses in cells of the same type across different recordings.

Second, variety in the eccentricity of the retinal pieces may have introduced additional diversity in the response properties. However, non-human primate studies investigating specific ganglion cell types tend to focus on a large proportion of the retina (e.g. 25-70 degrees in [24], 30-60 degrees in [16]), but did not report any significant differences in response properties across eccentricities.

Third, the health status could have altered the responses of the ganglion cells. On average, the human ganglion cells recorded here showed a similar response behavior to drifting-grating stimuli of different temporal and spatial frequencies as previously published non-human primate ganglion cells. The most abundant cell types in the primate retina are midget and parasol cells. Our dataset contains cells that responded similarly to drifting-grating stimuli as previously described midget and parasol cells in other primates. Although we have not performed chromatic testing, we recorded light responses that resembled a further abundant cell type in the primate retina, the small bistratified cells. Furthermore, the spatial threshold for the whole population of recorded cells (1.55 cyc/°) is comparable to psychophysically

determined spatial resolution thresholds of human subjects measured at comparable eccentricity. This, together with the absence of oscillations and the fact that we observed responding ganglion cells distributed across many recording electrodes, suggests that we were able to record physiologically relevant response properties in these donor human retinas.

Studies of primate retina often aim to characterize in detail a selected type of ganglion cell. In the present study, we considered all cells with light responses, and did not select for specific response features. This approach led to the characterization of response properties that have not been reported previously. While in other, non-human primates, cells responding to both positive and negative contrast (ON-OFF) have been readily described, the only other study that tested for contrast step responses in human ganglion cells concluded that there were only cells with ON- or OFF-type responses, but did not find any ON-OFF cells [28]. In our recordings, we found that 19% of all cells that responded to full-field contrast steps exhibited responses to both ON- and OFF-steps. Thus, while the presence of ON-OFF ganglion cells in human retina may not be entirely surprising, our study provides the first direct evidence for the existence of ON-OFF human retinal ganglion cells. In addition, while we recorded from cells that resembled the spatio-temporal response properties of parasol, midget-, and small bistratified cells (Fig. 5A and C), many of our human retinal ganglion cells had spatio-temporal response profiles that clearly differed from previously described primate ganglion cell types. For example, we recorded from broadly tuned cells that were activated strongly by all tested spatial frequencies ranging from 0.07 to 2.66 cyc/° (Fig. 5B). Such cells can inform the brain about aspects of the visual input independently of the size of the stimulus. Finally, the remaining cells showed a variety of specific temporal and spatial frequency tunings that do not correspond to the major ganglion cell types described in the non-human primate retina literature.

One of the best studied ganglion cells in non-primate mammalian retina are the direction-selective ganglion cells. It is unclear whether cells responding to a specific direction of

movement exist in the primate retina. So far, no physiological recordings of direction-selective cells have been published and we could not detect such direction-selective behavior in our data set either (data not shown). Morphological studies identified potential candidates for primate direction-selective neurons [48]. These cells have a large dendritic field and hence they are much fewer in number than the smaller midget or parasol cells. Consequently, the chances to record from such large cells in unbiased MEA experiments is small. Furthermore, as shown in the present study as well as in previous measurements [49], primate ganglion cells respond to higher temporal frequencies than for instance mouse ganglion cells [50]. It is therefore possible that our and other studies missed direction-selective cells in primate retinas due to suboptimal stimulation paradigms. This should be taken into consideration for future studies.

In this study we provide the first description of the retinal output in humans. We showed that our data is consistent with measurements in other primates and that the diversity in the human retinal output is much larger than suggested by previous physiological studies that focused on only a few primate retinal cell types. To further investigate these unstudied ganglion cells and to achieve classification into individual cell types, one could make use of high-density MEAs. These MEAs allow recording from almost every cell in a given patch [30], and local stimulation would be possible to test for parameters such as center-surround mechanisms, local edge detection or approach sensitivity. It has been shown that each ganglion cell type tiles the retina with little overlap in order to encode every visual feature at each point in the visual field [51]. Such mosaic formation can as well be revealed with high-density MEA recordings [15,16,22] and can then be used for cell type identification.

The goal of bio-medical research is to better understand human physiology and to find treatments in the case of disease. Knowledge about the detailed functioning of the human retina would be desirable also in the context of retinal diseases. Such diseases, in particular blindness, have a big impact on individuals and the society. In recent years, research has

yielded some promising approaches to potentially healing blindness (e.g. electrical retinal implants [52,53], optogenetics [54,55], stem cell therapy [56]) with a common ultimate goal: to come as close as possible to full vision capabilities by interfering appropriately with the retina of the patient. Especially optogenes (light sensitive ion channels/pumps) are a promising tool to render degenerated photoreceptors, bipolar cells, or ganglion cells light sensitive [54,55,57–59]. Currently, these treatment options are mostly developed and tested in animal models. We see a big advantage of supplementing this research with human retina studies. First, increased knowledge about signal processing within the human retina may support further and faster progress in that field. Second, cell type specificity of viral vectors and the correct expression of the genetic construct containing the optogenes could be developed using ex-vivo or post-mortem human retina. Moreover, by subsequent comparison of the optogene-driven light responses with the natural responses presented in this and future studies, one could evaluate the efficacy of the treatment. Finally, (side-)effects of drugs such as neuroprotectiva (substances to conserve as much as possible of leftover visual capabilities) could be tested directly on human retina instead of using porcine, bovine or other animal models. We thus hope that this study may serve as encouragement for more research with ex-vivo human retina in the future.

Methods

Human retina donations

To characterize information processing in the retina**,** very fresh tissue is necessary because the photoreceptors rapidly lose light-sensitivity. We obtained such human retina from patients of the University Eye Hospital in Tübingen, who had to undergo enucleation of one eye – usually to remove a tumor. All procedures were approved by the ethics committee of the University of Tuebingen (approval number 531/2011) and performed in accordance with the guidelines and regulations provided by the ethics committee. All participants provided

informed consent to the use of the removed retina for scientific research purposes. The retina was protected from light during surgery if possible. An ischemia time of at least five minutes during the surgery (clamping of the optic nerve before removing the bulbus) was mandatory to prevent strong bleeding. The bulbus was cut in halves directly after enucleation, and the hemisphere without tumor was put immediately into CO_2-independent culture medium (Gibco, ThermoFisher Scientific, Massachusetts, USA), kept in darkness at room temperature and transported to our lab. Under dim red light, we removed the vitreous and cut small mid-peripheral retinal pieces (~ 3x3 mm²). Within 23 months we obtained 15 such ex-vivo donations (Table 1). 15 pieces from 10 retinas were used for experiments. All procedures were reviewed and approved by the Ethics Committee of the University Clinic Tübingen.

Experimental design

To maximize the amount of information gained from the rare experiments with fresh human retina, we employed recordings with flat multi-electrode arrays (MEA) that allow for measuring the activity of many neurons in parallel [35]. MEAs include a square or rectangular electrode arrangement that is brought in contact with the ganglion cells, allowing measuring the retinal output in response to light stimulation. Our MEA experiments have been described in detail elsewhere [60]. Briefly, the retinal pieces were placed ganglion cell side-down on a MEA. We used perforated 60-electrode MEAs with 200 µm distance between the electrodes (60pMEA200/30iR-Ti-gr, Multichannel Systems, Reutlingen, Germany). Then, various light stimuli were focused onto the photoreceptors with a Digital Light Processing projector (Sharp PG-F212X-L, Sharp Corporation, Osaka, Japan or Acer K11, Acer, Taipeh, Taiwan), and we recorded the output of the retina (i.e. the action potentials of ganglion cells in response to the stimuli) at 25 kHz with a USB-MEA-system (USB-MEA1060, Multichannel Systems) or an MC-Card based MEA-system (MEA1060, Multichannel Systems). During the experiments, the retina was kept at 25°C and continuously superfused with Ringer solution (in mM: 110 NaCl, 2.5 KCl, 1 $CaCl_2$, 1.6 $MgCl_2$, 10 D-Glucose, and 22 $NaHCO_3$; ~270 mosm) or modified

Ringer solution (in mM: 115 NaCl, 2.5 KCl, 2 $CaCl_2$, 1 $MgCl_2$, 15 D-Glucose, 1.3 NaH_2PO_4*H_2O, 0.5 L-Glutamine, and 25 $NaHCO_3$; ~285 mosm), both equilibrated with carbogen (95% O_2, 5% CO_2). All experiments were conducted with the retinal pigment epithelium removed.

Light stimulation

The stimulation intensity provided by our projectors spanned 3 log units of brightness between a black ('0') and white ('255') stimulus. The projector output was linearized, so that the grey ('128') background was midway between black and white, and the intensity step between black and grey and between grey and white had equal amplitude. Recordings were performed at photopic intensity levels (light intensity for day vision) with a mean illuminance of $8 \cdot 10^4$ rod isomerizations per rod per second. In two retinal pieces, no clear responses could be detected at this light level, and we used data obtained at a mean illuminance of $8 \cdot 10^5$ rod isomerizations per rod per second for analysis. Note that recordings at photopic light levels do not necessarily imply that the observed light responses were driven by cones alone, rods may have contributed as well [61]. A broad set of light stimuli was used; each stimulus was repeated several times during recording sessions of two to six hours. We calculated various parameters from the ganglion cells' responses (see below). To convert stimulus sizes on the retina (in µm) to the equivalent visual angles (in degree), we used the conversion factor 266 µm/° [62]. We will discuss in this article six response parameters extracted from responses to the following six stimuli (see also Fig. 1):

<u>Sinusoidal drifting-gratings:</u> Drifting sinusoidal grating stimuli with 24 different combinations of spatial periods and temporal frequencies (1, 2, 4, 8 Hz; 100, 200, 500, 1000, 2000, 4000 µm spatial period on the retina) were used for spatio-temporal analysis (Fig. 1A). The gratings were shown at full contrast ('0' to '255') and moved in one direction for 12 seconds.

Temporal and contrast chirp: Temporal tuning was also tested with a spatially homogeneous chirp stimulus [2], i.e. full-field frequency-modulated intensity change between black (‘0) and white (‘255’), according to: intensity = $128 + 128 \sin(\pi (t^2 + t/10))$, with t given in seconds. The temporal frequency increased from 0.5 to 8 Hz over a time course of approximately 8 seconds (Fig. 1B top). In addition, a contrast ramp increasing from none to full contrast within 8 seconds was used to test for contrast sensitivity (Fig. 1B bottom).

Single bars at various velocities: We used single bars moving with different speed to test for speed preferences. A bar with 1000 µm extension in the movement direction (either black or white) moved in front of a gray background in one direction (same direction as grating stimulus) with different speeds (1, 2, 4, 8, 16 mm/s) with a gap of 3 seconds before the next higher speed (Fig. 1C).

Full-field contrast steps: Full-field contrast steps were applied for measurements of response polarity and latency (Fig. 1D). A single stimulus consisted of four transitions (grey → black → grey → white → grey) spanning the full projector intensity of 3 log units of brightness (contrast for each step: ± 1 Weber contrast). Each contrast step lasted for 2 seconds.

Direction-selectivity: We used a single bar (black or white) moving in 8 directions to test for direction-selectivity. The bar of 1000 µm width was moved with 1 mm/s across the retina.

Spike extraction

Spike sorting (assignment of single action potentials to individual cells) was performed with an in-house Matlab (MathWorks, Massachusetts, USA) routine written by Alexandra Tikidji-Hamburyan. Different features of the action potential waveforms, such as amplitude, width, or principal components, were calculated and projected onto 2-dimensional space to separate action potentials of different cells from each other and from noise. In addition, the spike refractory time of all spikes of a sorted cell had to be >1.5 ms. After spike sorting, we determined light-responding cells by visual inspection of the activity to all stimuli. To

calculate the firing rate, the spike train was convolved with a Gaussian and plotted against time. The sigma of the Gaussian varied for different analysis purposes; the value applied in each case is given in the description below. For the firing rates of the example cells in Figure 3, $\sigma = 40$ ms was used. Only cells for which spikes could be sorted confidently were used for analysis (for consistency, the same person performed spike sorting for all experiments and applied the identical quality judgement system). We applied cross-correlation analysis to detect recordings from the same cell on different electrodes (e.g. from cell body and axon). In this case, only one of the recorded units was used for the analysis.

Response parameter calculation

Spatio-temporal tuning: Drifting sinusoidal grating stimuli were used for spatio-temporal analysis. First, cells responding to at least one of the drifting gratings were identified manually. For each cell and stimulus repetition we represented the cell's activity with a binary vector indicating the presence (1) or absence (0) of a spike (time bins: 1 ms). For each drifting grating stimulus, we then calculated the mean of these binary spike rates and computed its Fourier transform (FT). The FT peak at the stimulus frequency was then taken as the cell's response strength. The Fourier transform was considered to have a peak (i.e., the cell was considered to respond to the stimulus) if there was no higher peak at any other frequencies (excluding multiples of the stimulus frequency).

Temporal tuning: Temporal tuning was tested with a chirp stimulus, i.e. frequency-modulated sinusoidal full-field change of intensity. We calculated the FT of both, the stimulus and the response (mean binary spike train, frequency resolution of 0.125 Hz). Response strength along the stimulation frequencies was defined as $\mathrm{norm}(FT_{response})/FT_{stimulus}$. Fluctuations were smoothed; these appeared especially at low temporal frequencies due to the timing of ON- and OFF-responses. Smoothing was achieved by averaging of the response strength with a moving average across a 3-datapoint-window (0.375 Hz) in steps of 1 data-point (0.125 Hz). Population data is presented in 2.6 Hz bins across all responding cells (Fig. 2C). As a second

method, temporal tuning was also calculated from the FT amplitudes obtained from the responses to drifting-grating stimuli.

Median speed preference: A black or white bar was moved across the retina in one direction (same direction as drifting granting) with various speeds. The cumulative sum of peak responses for each speed (firing rate calculated with σ = 40 ms) was computed. The speed value for which 50% of the cumulative sum was reached was taken as the cells' median speed preference. For each cell that responded to both, white and black bars, the higher preferred speed was taken for the population plot in Figure 2D.

Polarity: Polarity was defined based on the responses to full-field contrast steps. Cells with responses only for positive contrast steps were considered as ON-cells; OFF-cells had only detectable responses to negative contrasts, and ON-OFF-cells responded to both types of contrast steps. Firing rates were calculated by convolving the spike rates with a Gaussian (σ = 40 ms). The cell was considered to show a response if the peak firing rate was bigger than mean spontaneous activity + 2 standard deviations (measured before the first step in contrast).

Grouping of human ganglion cells: We aimed at identifying ganglion cells in our data set that resembled known primate retinal ganglion cell types. The only consistent description of response properties of non-human primate ganglion cells across different publications are spatial and temporal tuning curves. We thus computed spatial and temporal response curves based on the responses to the drifting sinusoidal grating stimuli:

Spatial response curve: For each cell, we summed the responses to each temporal frequency to identify the optimal stimulation frequencies. We then considered only the responses to all spatial frequencies tested at the optimal temporal frequency. The response strengths at that temporal frequency (along the 6 spatial frequencies) were considered the spatial tuning curve for the cell.

Temporal response curve: The temporal response curve was calculated in the same way as the spatial response curve. For each cell, we summed the responses to each spatial frequency and

considered only the spatial frequency with the maximal summed response for further analysis. The response strengths to the 4 temporal frequencies tested at this optimal spatial frequency were considered the cell's temporal response curve.

For further analysis, we normalized each tuning curve, calling the maximal response 100%. Note that the heatmaps in Figure 4 and 5 depict the mean of the individual cell's heatmaps, whereas the spatial and temporal response curves were generated based on the optimal temporal and spatial frequencies as described above. The mean response curves can hence not be extracted directly from the mean heatmaps.

The following criteria were applied to identify groups of ganglion cells:

Parasol/midget ganglion cells: A cell was considered for this group of cells resembling parasol/midget cells if it fulfilled the following criteria: (1) the response strength to gratings with 200 µm spatial period was > 40%, while the response strength to 100 µm gratings was < 20%. (2) The response to 1 and 2 Hz gratings was > 20%, and the responses to 4 and 8 Hz gratings were > 30%.

Blue-yellow ganglion cells: A cell was considered resembling blue-yellow cells if it fulfilled the following criteria: (1) the response to gratings with 100 and 200 µm spatial period was < 20%. (2) The response to 1 and 2 Hz gratings were > 20%, and the responses to 4 and 8 Hz gratings were > 30%. Note that our stimulus set did not contain color stimuli.

Broadly responding cells: A cell was considered a broadly responding cell if it fulfilled the following criteria: the responses for gratings with 100 and 200 µm spatial period were > 20%.

<u>Stability of spontaneous activity and contrast step responses:</u> Firing rates were calculated as described by Uzzell & Chichilnisky [44]. Briefly, recorded spikes were binned in 0.1 ms bins and smoothed with a Gaussian filter with a sigma of 2 ms. The firing rates for 5 consecutive full-field contrast step stimuli were averaged and the peak response amplitude was extracted. Similarly, the mean firing rate of the 1.7 seconds before the first step in contrast was used to

track spontaneous firing rates during the experiment. The firing rates of the example cell in Figure 6C_2 were calculated using $\sigma = 60$ ms.

References

1. Lettvin, J. Y., Maturana, H. R., Maturana, H. R., Mcculloch, W. S. & Pitts, W. H. What the Frog's Eye Tells the Frog's Brain. *Proc. IRE* **47,** 1940–1951 (1959).
2. Baden, T. *et al.* The functional diversity of mouse retinal ganglion cells. *Nature* **529,** 1–21 (2016).
3. Sanes, J. R. & Masland, R. H. The types of retinal ganglion cells: current status and implications for neuronal classification. *Annu. Rev. Neurosci.* **38,** 221–46 (2015).
4. Farrow, K. & Masland, R. H. Physiological clustering of visual channels in the mouse retina. *J. Neurophysiol.* **105,** 1516–1530 (2011).
5. Devries, S. H. & Baylor, D. A. Mosaic arrangement of ganglion cell receptive fields in rabbit retina. *J. Neurophysiol.* **78,** 2048–2060 (1997).
6. Wong, R. C., Cloherty, S. L., Ibbotson, M. R. & O'Brien, B. J. Intrinsic physiological properties of rat retinal ganglion cells with a comparative analysis. *J. Neurophysiol.* **108,** 2008–2023 (2012).
7. Marre, O. *et al.* Mapping a complete neural population in the retina. *J. Neurosci.* **32,** 14859–14873 (2012).
8. Polyak, S. L. *The Retina*. (The University of Chicago, 1941).
9. Kaplan, E. & Shapley, R. M. The primate retina contains two types of ganglion cells, with high and low contrast sensitivity. *Proc. Natl. Acad. Sci. U. S. A.* **83,** 2755–7 (1986).
10. Rodieck, R. W., Binmoeller, K. F. & Dineen, J. Parasol and midget ganglion cells of the human retina. *J. Comp. Neurol.* **233,** 115–132 (1985).
11. Dacey, D. M. in *The Cognitive Neurosicences* 281–301 (2004).
12. Chichilnisky, E. J. & Kalmar, R. S. Functional asymmetries in ON and OFF ganglion cells of primate retina. *J. Neurosci.* **22,** 2737–47 (2002).
13. Dacey, D. M. & Brace, S. A coupled network for parasol but not midget ganglion cells in the primate retina. *Vis. Neurosci.* **9,** 279–290 (1992).
14. Dacey, D. M. & Lee, B. B. The 'blue-on' opponent pathway in primate retina originates from a distinct bistratified ganglion cell type. *Nature* **367,** 731–735 (1994).
15. Gauthier, J. L. *et al.* Uniform Signal Redundancy of Parasol and Midget Ganglion Cells in Primate Retina. *J. Neurosci.* **29,** 4675–4680 (2009).
16. Greschner, M. *et al.* Correlated firing among major ganglion cell types in primate retina. *J. Physiol.* **589,** 75–86 (2011).
17. Shlens, J. *et al.* The Structure of Large-Scale Synchronized Firing in Primate Retina. *J. Neurosci.* **29,** 5022–5031 (2009).
18. Doi, E. *et al.* Efficient Coding of Spatial Information in the Primate Retina. *J. Neurosci.* **32,** 16256–16264 (2012).
19. Field, G. D. & Chichilnisky, E. J. Information Processing in the Primate Retina: Circuitry and Coding. *Annu. Rev. Neurosci.* **30,** 1–30 (2007).
20. Peterson, B. B. & Dacey, D. M. Morphology of human retinal ganglion cells with

intraretinal axon collaterals. *Vis. Neurosci.* **15,** 377–87 (1998).

21. YAMADA, E. S., BORDT, A. S. & MARSHAK, D. W. Wide-field ganglion cells in macaque retinas. *Vis. Neurosci.* **22,** 383–393 (2005).

22. Petrusca, D. *et al.* Identification and characterization of a Y-like primate retinal ganglion cell type. *J. Neurosci.* **27,** 11019–27 (2007).

23. Chichilnisky, E. J. & Baylor, D. A. Receptive-field microstructure of blue-yellow ganglion cells in primate retina. *Nat. Neurosci.* **2,** 889–893 (1999).

24. Field, G. D. *et al.* Spatial Properties and Functional Organization of Small Bistratified Ganglion Cells in Primate Retina. *J. Neurosci.* **27,** 13261–13272 (2007).

25. Dacey, D. M. *et al.* Melanopsin-expressing ganglion cells in primate retina signal colour and irradiance and project to the LGN. *Nature* **433,** 749–754 (2005).

26. De Monasterio, F. M. & Gouras, P. Functional properties of ganglion cells of the rhesus monkey retina. *J. Physiol.* **251,** 167–95 (1975).

27. Schiller, P. H. & Malpeli, J. G. Properties and tectal projections of monkey retinal ganglion cells. *J. Neurophysiol.* **40,** 428–45 (1977).

28. Hashimoto, T., Katai, S., Saito, Y., Kobayashi, F. & Goto, T. ON and OFF channels in human retinal ganglion cells. *J. Physiol.* **591,** 327–337 (2013).

29. Weinstein, G. W., Hobson, R. R. & Baker, F. H. Extracellular recordings from human retinal ganglion cells. *Science* **171,** 1021–2 (1971).

30. Fiscella, M. *et al.* Recording from defined populations of retinal ganglion cells using a high-density CMOS-integrated microelectrode array with real-time switchable electrode selection. *J. Neurosci. Methods* **211,** 103–113 (2012).

31. Frey, U., Egert, U., Heer, F., Hafizovic, S. & Hierlemann, A. Microelectronic system for high-resolution mapping of extracellular electric fields applied to brain slices. *Biosens. Bioelectron.* **24,** 2191–8 (2009).

32. Segev, R., Goodhouse, J., Puchalla, J. & Berry, M. J. Recording spikes from a large fraction of the ganglion cells in a retinal patch. *Nat. Neurosci.* **7,** 1154–61 (2004).

33. Zeck, G. M. & Masland, R. H. Spike train signatures of retinal ganglion cell types. *Eur. J. Neurosci.* **26,** 367–380 (2007).

34. Meister, M., Lagnado, L. & Baylor, D. A. Concerted signaling by retinal ganglion cells. *Science* **270,** 1207–10 (1995).

35. Meister, M., Pine, J. & Baylor, D. A. Multi-neuronal signals from the retina: acquisition and analysis. *J. Neurosci. Methods* **51,** 95–106 (1994).

36. Rovamo, J., Virsu, V. & Näsänen, R. Cortical magnification factor predicts the photopic contrast sensitivity of peripheral vision. *Nature* **271,** 54–6 (1978).

37. Diller, L. *et al.* L and M cone contributions to the midget and parasol ganglion cell receptive fields of macaque monkey retina. *J. Neurosci.* **24,** 1079–88 (2004).

38. CROOK, J. D., PACKER, O. S. & DACEY, D. M. A synaptic signature for ON- and OFF-center parasol ganglion cells of the primate retina. *Vis. Neurosci.* **31,** 57–84 (2014).

39. Crook, J. D. *et al.* Parallel ON and OFF Cone Bipolar Inputs Establish Spatially Coextensive Receptive Field Structure of Blue-Yellow Ganglion Cells in Primate Retina. *J. Neurosci.* **29,** 8372–8387 (2009).

40. DACEY, D. M., CROOK, J. D. & PACKER, O. S. Distinct synaptic mechanisms create parallel S-ON and S-OFF color opponent pathways in the primate retina. *Vis. Neurosci.* **31,** 139–151 (2014).

41. Crook, J. D., Packer, O. S. & Dacey, D. M. A synaptic signature for ON- and OFF-

center parasol ganglion cells of the primate retina. *Vis. Neurosci.* **31,** 57–84 (2014).

42. Reinhard, K. *et al.* Hypothermia Promotes Survival of Ischemic Retinal Ganglion Cells. *Investig. Opthalmology Vis. Sci.* **57,** 658 (2016).

43. Menzler, J. & Zeck, G. Network Oscillations in Rod-Degenerated Mouse Retinas. *J. Neurosci.* **31,** 2280–2291 (2011).

44. Uzzell, V. J. & Chichilnisky, E. J. Precision of Spike Trains in Primate Retinal Ganglion Cells. *J. Neurophysiol.* **92,** 780–789 (2004).

45. Farrow, K. *et al.* Ambient illumination toggles a neuronal circuit switch in the retina and visual perception at cone threshold. *Neuron* **78,** 325–338 (2013).

46. Field, G. D. *et al.* High-sensitivity rod photoreceptor input to the blue-yellow color opponent pathway in macaque retina. *Nat. Neurosci.* **12,** 1159–64 (2009).

47. Tikidji-Hamburyan, A. *et al.* Retinal output changes qualitatively with every change in ambient illuminance. *Nat. Neurosci.* **18,** 66–74 (2015).

48. Moritoh, S., Komatsu, Y., Yamamori, T. & Koizumi, A. Diversity of Retinal Ganglion Cells Identified by Transient GFP Transfection in Organotypic Tissue Culture of Adult Marmoset Monkey Retina. *PLoS One* **8,** e54667 (2013).

49. Lee, B. B., Pokorny, J., Smith, V. C. & Kremers, J. Responses to pulses and sinusoids in macaque ganglion cells. *Vision Res.* **34,** 3081–96 (1994).

50. Grubb, M. S. & Thompson, I. D. Visual Response Properties of Burst and Tonic Firing in the Mouse Dorsal Lateral Geniculate Nucleus. *J. Neurophysiol.* **93,** 3224–3247 (2005).

51. Wässle, H. & Riemann, H. J. The mosaic of nerve cells in the mammalian retina. *Proc. R. Soc. London. Ser. B, Biol. Sci.* **200,** 441–61 (1978).

52. Dorn, J. D. *et al.* The Detection of Motion by Blind Subjects With the Epiretinal 60-Electrode (Argus II) Retinal Prosthesis. *JAMA Ophthalmol.* **131,** 183 (2013).

53. Zrenner, E. *et al.* Subretinal electronic chips allow blind patients to read letters and combine them to words. *Proc. R. Soc. B Biol. Sci.* **278,** 1489–1497 (2011).

54. Busskamp, V. & Roska, B. Optogenetic approaches to restoring visual function in retinitis pigmentosa. *Curr. Opin. Neurobiol.* **21,** 942–946 (2011).

55. Lagali, P. S. *et al.* Light-activated channels targeted to ON bipolar cells restore visual function in retinal degeneration. *Nat. Neurosci.* **11,** 667–675 (2008).

56. Tibbetts, M. D., Samuel, M. A., Chang, T. S. & Ho, A. C. Stem cell therapy for retinal disease. *Curr. Opin. Ophthalmol.* **23,** 226–34 (2012).

57. Bi, A. *et al.* Ectopic Expression of a Microbial-Type Rhodopsin Restores Visual Responses in Mice with Photoreceptor Degeneration. *Neuron* **50,** 23–33 (2006).

58. Mutter, M. & Münch, T. A. Strategies for Expanding the Operational Range of Channelrhodopsin in Optogenetic Vision. *PLoS One* **8,** e81278 (2013).

59. van Wyk, M., Pielecka-Fortuna, J., Löwel, S. & Kleinlogel, S. Restoring the ON Switch in Blind Retinas: Opto-mGluR6, a Next-Generation, Cell-Tailored Optogenetic Tool. *PLOS Biol.* **13,** e1002143 (2015).

60. Reinhard, K. *et al.* Step-By-Step Instructions for Retina Recordings with Perforated Multi Electrode Arrays. *PLoS One* **9,** e106148 (2014).

61. Tikidji-Hamburyan, A. *et al.* Rods progressively escape saturation to drive visual responses in daylight conditions. *Nat. Commun.* **8,** 1813 (2017).

62. Drasdo, N. & Fowler, C. W. Non-linear projection of the retinal image in a wide-angle schematic eye. *Br. J. Ophthalmol.* **58,** 709–14 (1974).

Additional information

Conflict of interest

The authors declare no conflict of interest.

Acknowledgements

We thank Prof. Karl Ulrich Bartz-Schmidt and the surgery team of the University Clinics Tübingen for the support during the human retina donation process. We further thank Dr. Hartwig Seitter (University of Innsbruck, Austria), Dr. Boris Benkner, Marion Mutter, and Natalia Świętek for technical support; Dr. Alexandra Tikidji-Hamburyan (Stanford University, California, USA) for the spike-sorting code; and Dr. Karl Farrow and Dr. Vincent Bonin (both NERF, Leuven, Belgium) for helpful comments on the manuscript. This research was supported by funds of the Deutsche Forschungsgemeinschaft (DFG) to the Werner Reichardt Centre for Integrative Neuroscience (DFG EXC 307), by the Bundesministerium für Bildung and Forschung (BMBF) to the Bernstein Center for Computational Neuroscience (FKZ 01GQ1002), a Pro-Retina Stipend to KR, and the Lush Prize 2015 for young investigators to KR.

Author Contributions

KR and TAM designed the study and the experiments. KR performed the experiments and analyzed the data. KR and TAM wrote the manuscript.

Table 1: Human retinas used for this study.

Donor				Surgery conditions		Retina		Experiment notes		
ID	Sex	Age	Notes	Ischemia (min)	Dark lens	Eye	Retinal part (ventr./dors./ temp./nasal)	Preparation	# Analyzed pieces	Any light resp.?
1	m	72	diabetic	7	-	right	vt	easy	1	yes
2	f	49	***radiation***	7	-	right	dn		-	-
3	f	72	diabetic	7	-	left	dn	rolling	1	yes
4	f	69	detachment	17	-	left	n	easy	1	yes
5	m	53		7	-	left	t	sticky	1	yes
***6**	m	75	sinus tumor	***18***	-				-	-
7	m	89		***25***	-	right	dn	sticky	-	yes
8	f	42		***20***	-	left	vt	sticky	-	-
9	f	83		10	-	right	t	sticky	1	yes
10	f	49		10	-	left	t	sticky	3	yes
11	f	60		7	yes	left	vn	sticky	3	yes
12	f	74	macular edema	7	yes	left	dt	easy	2	yes
13	m	74		7	yes	left	v	***very sticky***	-	yes
14	f	79	radiation 10y ago	8	-	left	n	easy	1	yes
15	m	67	detachment	10	-	left	n	easy	1	yes

15 ex-vivo human retinas were obtained. The table contains information about the donor (sex, age, known medical history), surgery conditions (the ischemia duration, i.e. time without oxygen and nutrient supply, and whether a dark lens was put on the donor's eye during surgery), and the retina (left/right eye, part of the retina without tumor). During preparation, the retina would sometimes roll up immediately after vitrectomy (rolling) or the vitreous was sticking strongly to the retina (sticky). The last two columns indicate how many retinal pieces were used per retina for the final analysis and whether any light responses were detected in our recordings. Light gray rows: retinas with few light responses, not used for analysis. Dark gray rows: no detectable light responses. Bold: potential reasons for low quality. Ventr./v = ventral, dors./d = dorsal, temp./t = temporal, n = nasal, m = male, f = female, radiation = radiation of the tumor-bearing eye, detachment = partial retinal detachment prior to surgery, resp. = responses. *retina prepared by another group during a different study.

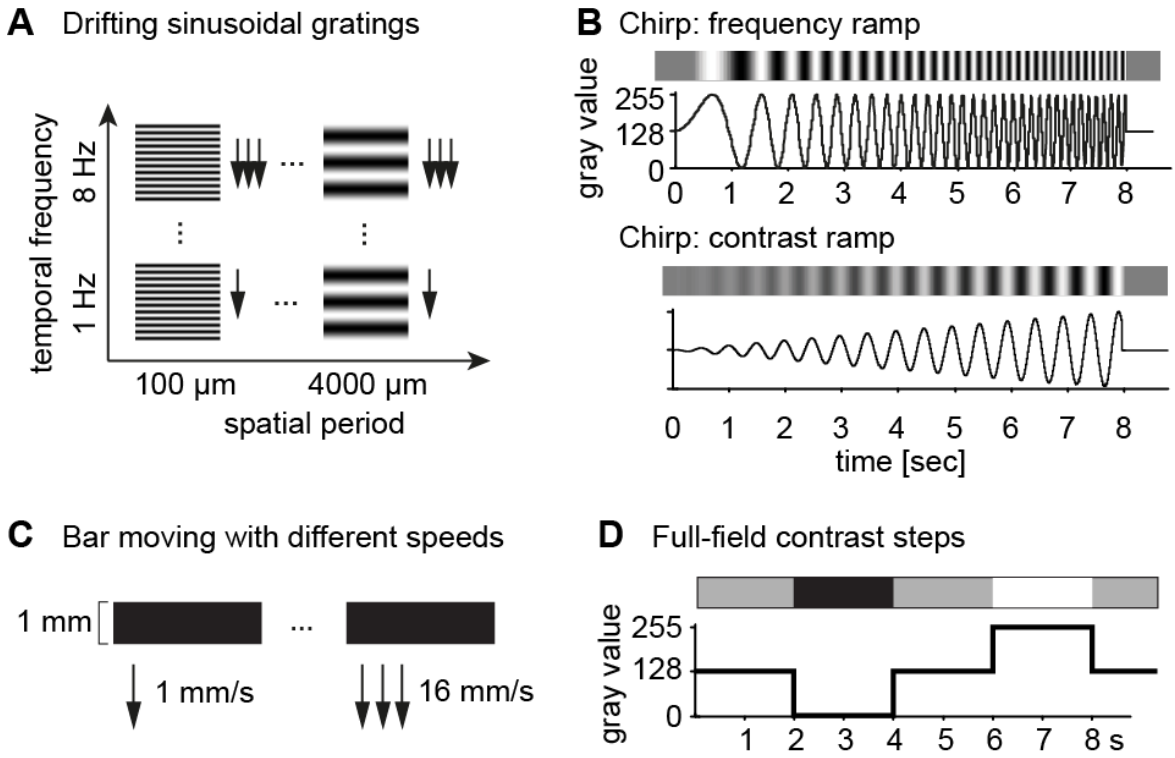

Figure 1: Light stimuli. A) Drifting gratings with 4 temporal frequencies and 6 spatial frequencies. B) Full-field "chirp" frequency ramp from 0.5 to 8 Hz and full-field "chirp" contrast ramp. C) Bar moving with 6 different speeds. D) Full-field flash contrast steps consisting of two positive and two negative contrast steps.

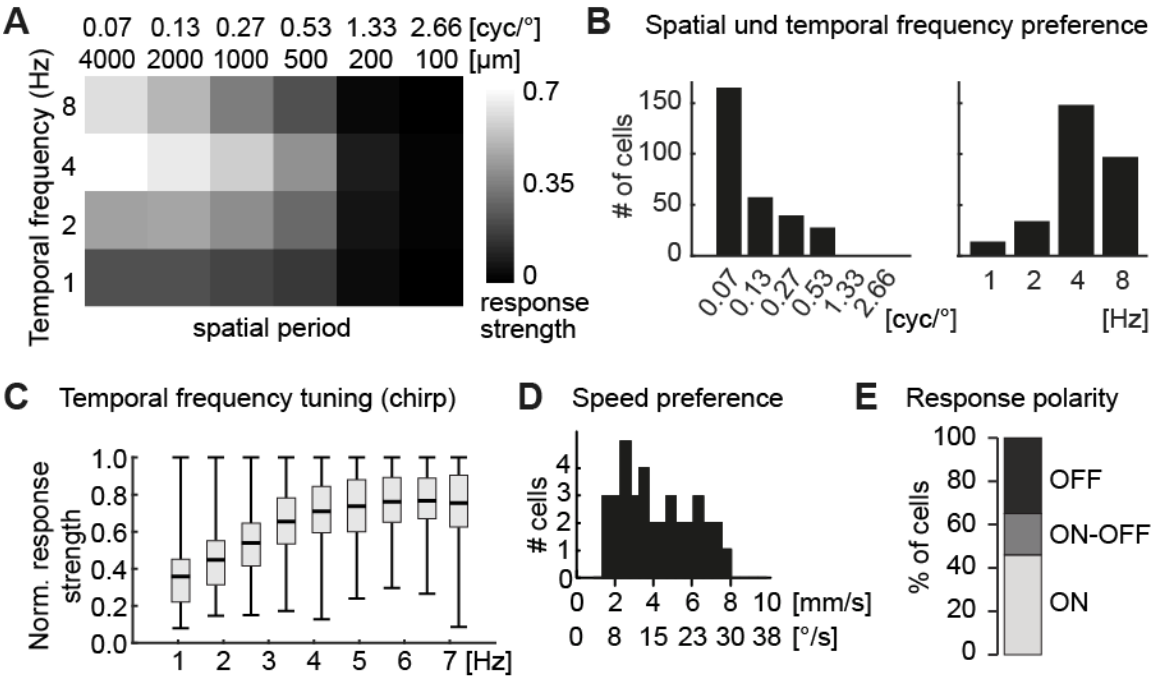

Figure 2: Characteristics of the human retinal output. (A) Response strength (amplitude of the Fourier Transform (FT) normalized to maximal response) to 24 drifting sinusoidal gratings with different spatial and temporal frequencies, averaged across N = 293 cells. (B) Distribution of preferred spatial (left) and temporal (right) frequencies in response to drifting gratings, N = 293 cells. (C) Normalized response strength ($FT_{response}/FT_{stimulus}$) to a full-field frequency ramp ("chirp"), in different frequency bands (Box-whisker-plots: mean, quartiles, maximum and minimum; N = 141 cells). (D) Distribution of the median preferred speed measured with a single moving bar, N = 37 cells. (E) Proportion of ganglion cells responding to positive full-field contrast steps (ON), negative contrast steps (OFF) or both (ON-OFF), N = 121 cells.

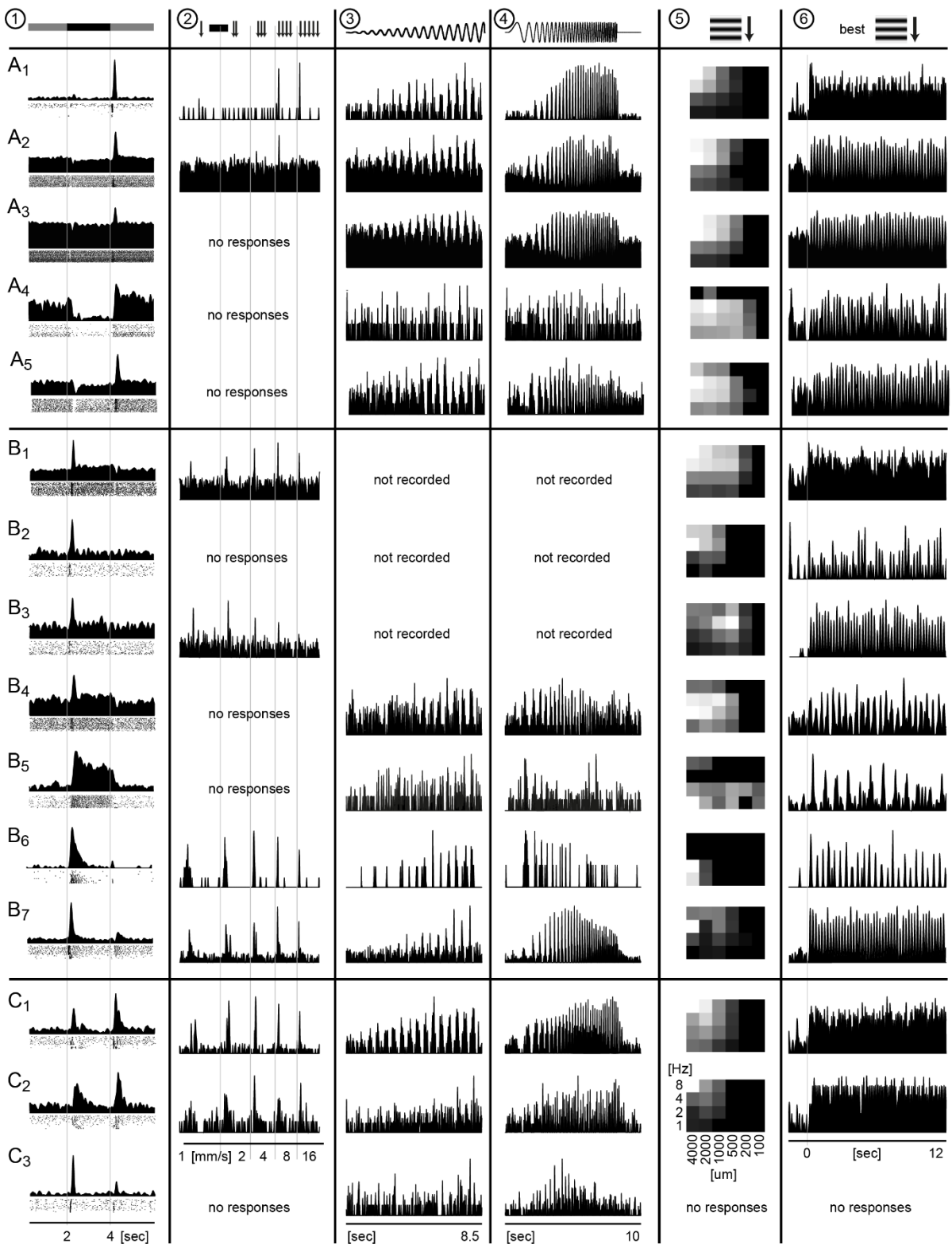

Figure 3: Example response properties of human ganglion cells. A) ON-cells, B) OFF-cells, C) ON-OFF-cells. Column 1: average firing rates (top) and raster plots (bottom) to full-field contrast steps; column 2: response to bar moving with different speeds; column 3: activity during a full-field contrast ramp at 2 Hz; column 4: response to "chirp stimulus" (full-field temporal frequency modulation from 0.5 to 8 Hz); column 5: normalized response strengths to 24 sinusoidal drifting-gratings; column 6: firing rate for sinusoidal drifting-grating with maximal response (white square in column 5). Stimuli are depicted on top.

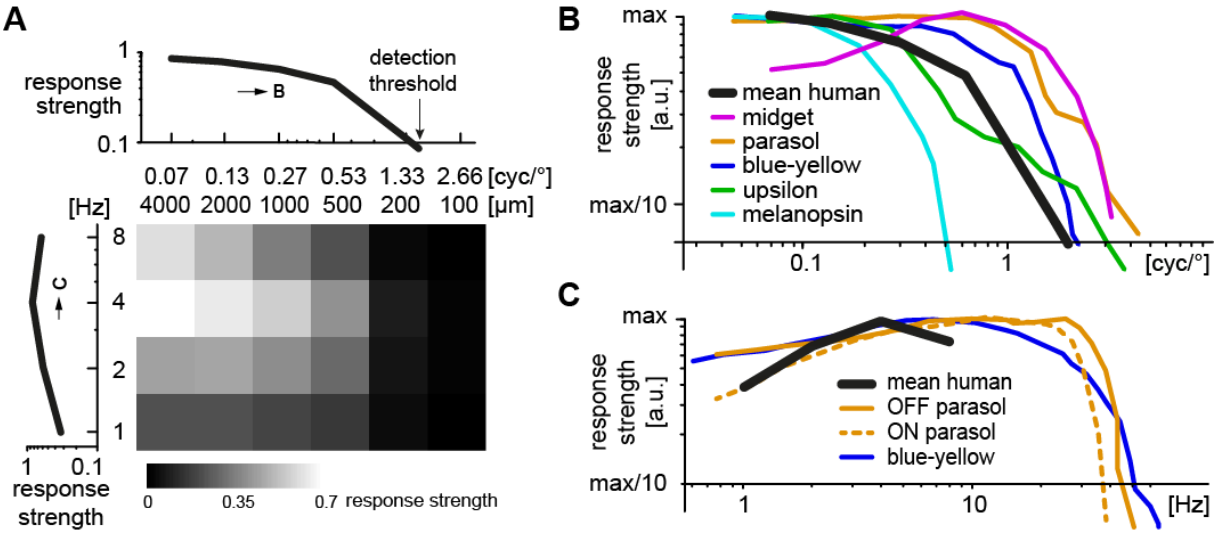

Figure 4: Human retinal ganglion cells show similar spatial and temporal frequency response curves as non-human primate retinal ganglion cells. (A) Heat map: Average responsivity of human retinal ganglion cells for drifting sinusoidal gratings, replicated from Fig. 2A (N = 293). Curves: Spatial frequency (top) and temporal frequency (left) response curves (mean across all cells). (B, C) Spatial and temporal response curve in comparison with published data on non-human primate ganglion cells. Non-human primate data adapted from Diller et al. 2004 (midget); Crook et al. 2009, 2014 (parasol); Crook et al. 2009, Dacey et al. 2014 (blue-yellow); Petrusca et al. 2007 (upsilon); Dacey et al. 2005 (melanopsin).

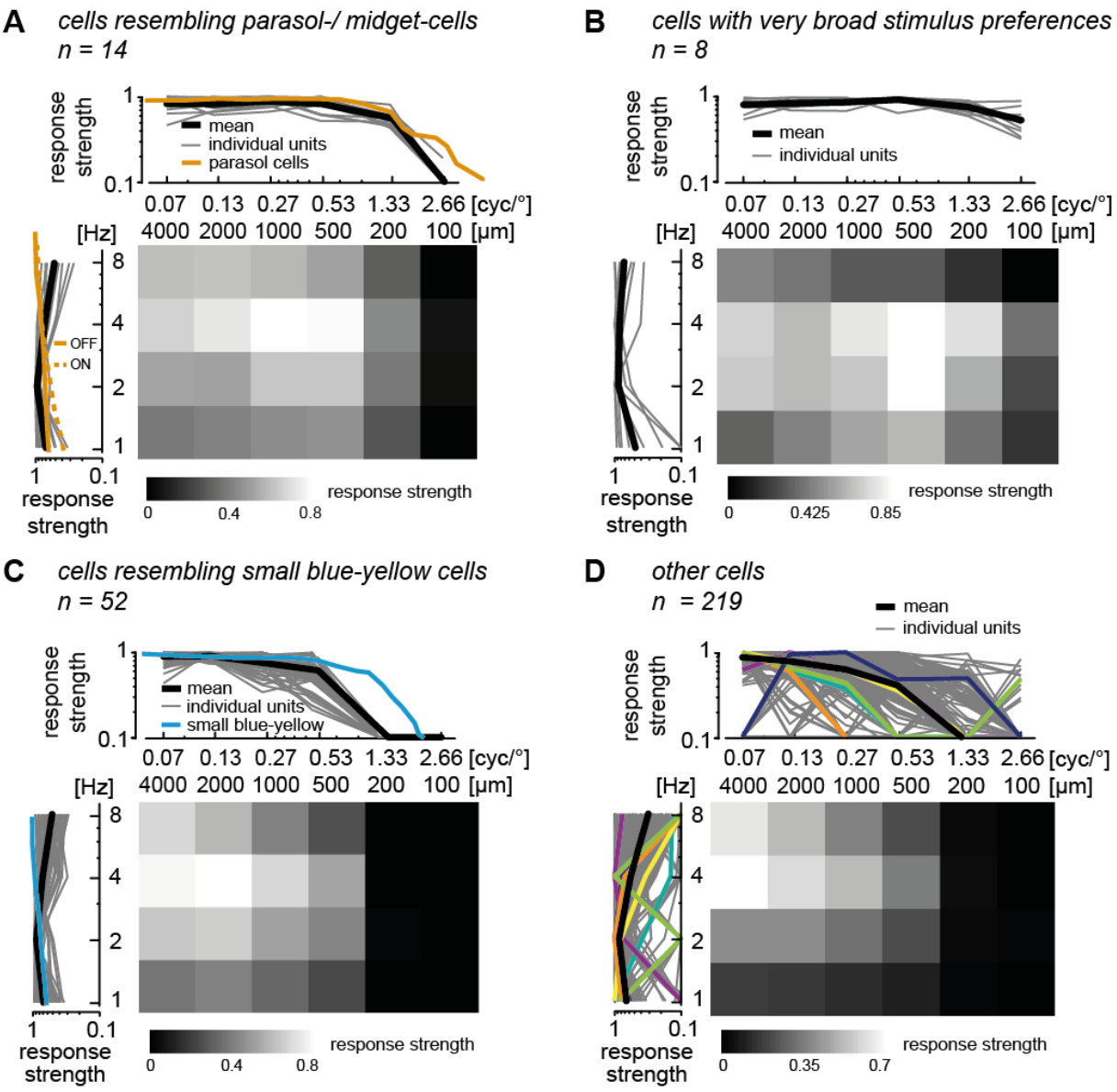

Figure 5: Groups of human retinal ganglion cells with similar properties. (A) Cells resembling parasol or midget cells. (B) Broadly responding cells. (C) Cells resembling small blue-yellow cells. (D) Remaining cells. 5 individual cells are emphasized in color to highlight the diversity in this group.

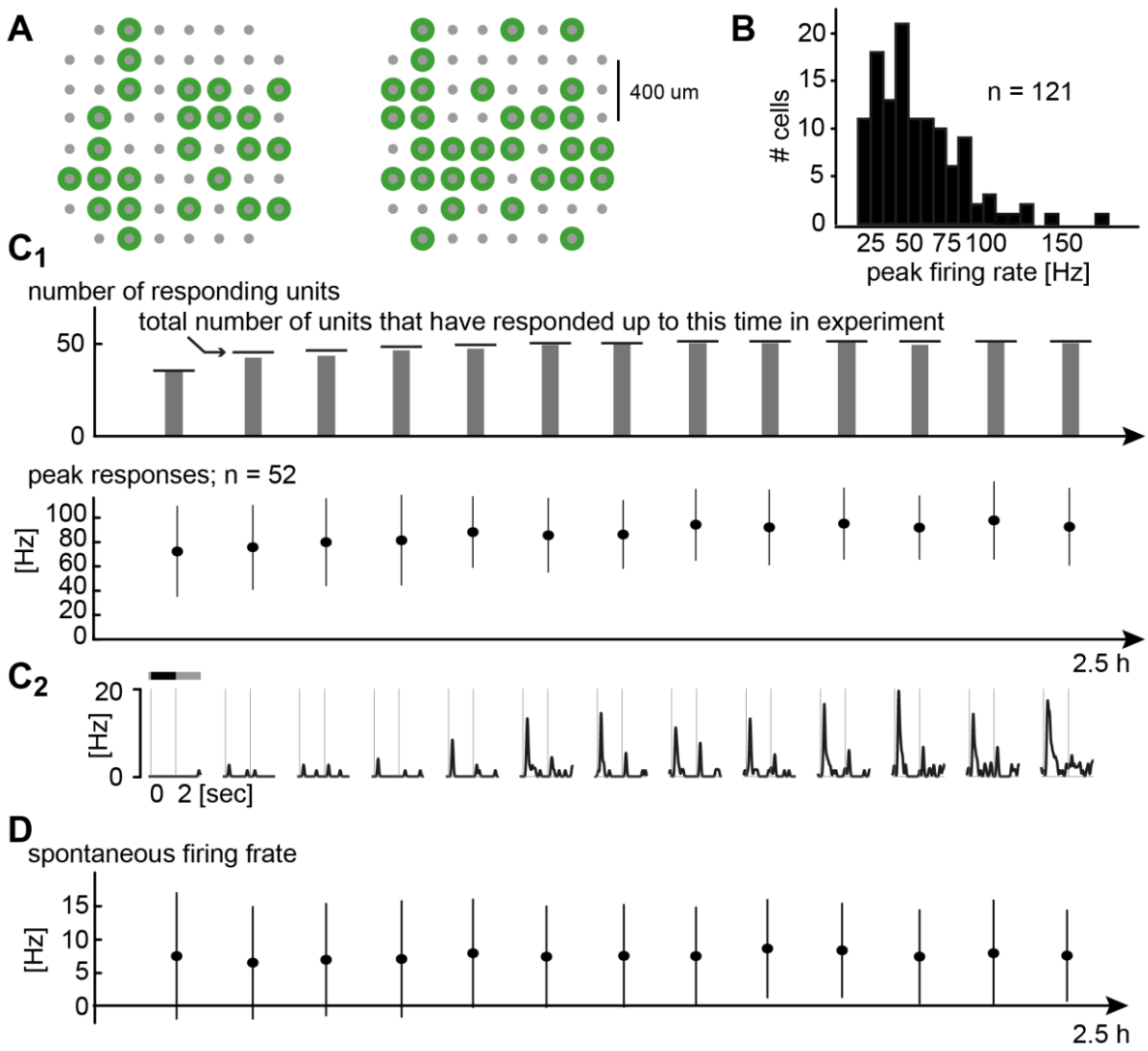

Figure 6: Donated human retinas are healthy. (A) Multi-electrode array layout (gray) and electrodes with sortable, light-responsive cells (green) of two example experiments. Responding cells are distributed across the recorded retinal pieces. (B) Distribution of peak firing rates in response to full-field contrast steps. (C_1) Top: Number of cells responding at any given time point (gray bars) was similar to the total number that had responses until that time point (horizontal lines). Bottom: Mean ± standard deviation of peak firing rate for the responding cells. Data from a subset of experiments that lasted for 2.5h (N = 4 experiments, N= 52 cells). (C_2) Example firing rate traces for one cell. (D) Spontaneous background firing rates (mean ± standard deviation) of the same cells and time points as in C_1.